Theoretical Simulation of n-Alkane Cracking on Zeolites

Joseph A. Swisher,[†,||] Niels Hansen,[‡,||] Theo Maesen,[§] Frerich J. Keil,[‡] Berend Smit,*[,†] and Alexis T. Bell*[,†]

Department of Chemical Engineering, University of California, Berkeley, California 94720-1462, Department of Chemical Engineering, Hamburg University of Technology, D-21073 Hamburg, Germany, and Chevron Energy Technology Company, 100 Chevron Way, Richmond, California 94801-2016

Received: February 9, 2010; Revised Manuscript Received: April 26, 2010

The kinetics of alkane cracking in zeolites MFI and FAU have been simulated theoretically from first principles. The apparent rate coefficient for alkane cracking was described as the product of the number of alkane molecules per unit mass of zeolite that are close enough to a Brønsted-acid site to be in the reactant state for the cleavage of a specific C−C bond and the intrinsic rate coefficient for the cleavage of that bond. Adsorption thermodynamics were calculated by Monte Carlo simulation and the intrinsic rate coefficient for alkane cracking was determined from density functional theory calculations combined with absolute rate theory. The effects of functional, basis set, and cluster size on the intrinsic activation energy for alkane cracking were investigated. The dependence of the apparent rate coefficient on the carbon number for the cracking of C_3-C_6 alkanes on MFI and FAU determined by simulation agrees well with experimental observation, but the absolute values of the apparent rate coefficients are a factor of 10 to 100 smaller than those observed. This discrepancy is attributed to the use of a small T5 cluster representation of the Brønsted-acid site. Limited calculations for propane and butane cracking on MFI reveal that significantly better agreement between prediction and observation is achieved using a T23 cluster for both the apparent rate coefficient and the apparent activation energy. The apparent rate coefficients for alkane cracking are noticeably larger for MFI than FAU, in agreement with recent findings reported in the experimental literature.

Introduction

A long-standing goal of theoretical studies in the field of heterogeneous catalysis has been the development of methods to predict the effects of catalyst composition and structure on the rates of catalyzed reactions, as well as the distribution of the products formed from a specified set of reactants. Impressive progress toward this goal has been made during the past two decades, resulting in a much better understanding of the various factors contributing to the rates of catalyzed reactions. For example, it is now possible to predict adsorption isotherms and diffusion coefficients for various molecules and mixtures of molecules in zeolites of different framework structure and pore size using the methods of statistical mechanics and molecular dynamics.[1,2] Likewise quantum chemical calculations, particularly those based on density functional theory (DFT), have advanced to a stage where it is possible to analyze complex reaction pathways and to calculate rate coefficients for elementary processes.[3−8] In a number of instances, it has been demonstrated that overall reaction kinetics determined using such rate coefficients correctly describe observed rates and changes with catalyst composition.[9−12] These successes suggest that by combining different theoretical methods, it should be possible to make quantitative predictions of reaction kinetics for systems involving the combined effects of reaction kinetics, adsorption, and diffusion. The initial efforts in this direction are encouraging, and, hence, it is anticipated that theoretical investigation of the combined effects of adsorption thermodynamics, diffusion, and reaction kinetics on the rates of catalyzed reactions will continue to be a fertile area for future research.

The cracking of alkanes at Brønsted-acid centers in zeolites is a reaction of central importance in the production of fuels from petroleum. While this process has been studied for over 60 years, the reaction mechanism and kinetics and the effects of zeolite framework structure on the rate of alkane cracking remain subjects of discussion.[13] There is consensus, however, that alkanes are first adsorbed into the pore space of the zeolite and then undergo cracking at Brønsted-acid sites.

The product distributions observed for zeolite-catalyzed cracking of light alkanes were originally rationalized using the classical or bimolecular cracking mechanism proposed by Greensfelder et al.[14] and Thomas[15] in 1949. Carbenium ions were thought to be formed by the adsorption of small amounts of alkenes present in the feed. It was hypothesized that these cations then abstract a hydride anion from the alkane reactant and the resulting carbenium cation then rapidly rearranges via beta scission to form an alkene and a smaller carbenium ion. Subsequent work by Haag and Dessau[16] observed that the classical mechanism did not explain the product distributions observed for the cracking of hexane isomers at high temperature and proposed, instead, the protolytic or monomolecular mechanism. They suggested that five-coordinate alkanium ions (formerly referred to as carbonium ions) are formed via protonation of alkanes by Brønsted-acid sites in the zeolite. The alkanium cations decompose to produce hydrogen or an alkane, for example, methane, ethane, and a carbenium ion. The latter species undergoes β-elimination of a proton to form an alkene and a Brønsted-acid site. As discussed in the reviews by Gates and co-workers[17,18] it is now recognized that both mono- and

* To whom correspondence should be addressed. E-mail: (B.S.) berend-smit@berkeley.edu; (A.T.B) bell@cchem.berkeley.edu.
† University of California.
‡ Hamburg University of Technology.
§ Chevron Energy Technology Company.
|| These authors contributed equally to this work.

10.1021/jp101262y
Published on Web 05/14/2010

bimolecular mechanisms of alkane cracking may be operative with the former predominating in small pore zeolites and at low alkane conversions. At high alkane conversions, alkenes react preferentially with Brønsted-acid protons and the bimolecular mechanism becomes the predominant reaction pathway.

The effects of alkane chain length and zeolite structure on the intrinsic rate of alkane cracking have also been the subject of numerous studies.[19−29] These efforts have focused on accurate measurement of reaction rates and adsorption thermodynamics with the aim of determining the intrinsic kinetic parameters for cracking and explaining the observed exponential dependence of apparent cracking rate on the number of carbon atoms in the alkane. It has been observed that alkane cracking activity increases with the heat of alkane adsorption and that the heat of adsorption for n-alkanes increases monotonically with carbon number.[25,28] It has also been noted that for a given carbon number the heat of adsorption increases with a decrease in the ratio of the diameter of the zeolite pores relative to the diameter of the alkane along its principal axis.[26] Correcting the apparent activation energy with the heat of adsorption has led to the conclusion that intrinsic activation energies are similar for all zeolites studied, suggesting that the activity of Brønsted-acid sites in different frameworks are comparable.[19,27] This conclusion has recently been questioned by Bhan et al.,[30] who have suggested that the intrinsic rate coefficient for alkane cracking is a function of zeolite structure.

The aim of the present study was to carry out a first-principles analysis of light alkane (C_3-C_6) cracking in order to predict quantitatively the turnover numbers for alkane cracking as a function of alkane carbon number and zeolite structure. The thermodynamics of propane, *n*-butane, *n*-pentane, and *n*-hexane adsorption in two zeolite structures were determined by molecular simulation for temperatures at which alkane cracking occurs. DFT calculations were performed to analyze the reaction pathway(s) for the cracking of each alkane and to determine the activation barrier for the rate-determining step. Single-point, MP2 calculations were conducted to assess how this higher level of theory compares with calculations done at the DFT. Rate coefficients were then determined for each step from absolute rate theory. The apparent rate coefficient was calculated as the product of the equilibrium coefficient for alkane adsorption, the equilibrium coefficient for the association of a specific C−C bond with a Brønsted-acid site, and the intrinsic rate coefficient for alkane cracking of the targeted C−C bond. Calculated rate coefficients determined in this manner were compared with those observed experimentally for the cracking of C_3-C_6 alkanes in MFI and FAU. The approach used in this study allowed us to address the causes for the observed differences in the reactivity of alkanes with increasing carbon number in a given zeolite and the differences in cracking activity with zeolite framework structure for a given alkane.

Theory

Kinetics of Alkane Cracking. In this work we consider the cracking of propane through hexane in Brønsted-acid zeolites with different framework structures and Si/Al ratios. As shown in Scheme 1, an alkane and an alkene are formed when each C−C bond is cracked. It is also seen that the number of products formed increases with the carbon number of the alkane. The acid sites at which these reactions occur are not all the same, each one being associated with a crystallographicly distinct T site. Therefore, the intrinsic rate coefficient for the cracking of an *n*-alkane, $k_{int}(i,j)$, depends on the type of acid site, *i*, and the reaction path, *j*. The rate at which reaction *j* occurs at site *i* is proportional to the average number of alkane molecules per unit zeolite mass that are close enough to an acid site, such that the alkane will undergo reaction *j*. This number, $\langle N_{react}(i,j,P_A,n_{Si/Al}(i))\rangle$, is function of the alkane partial pressure, P_A, and the number of acid sites of type *i* per unit zeolite mass, $n_{Si/Al}(i)$. It should be noted that the sum over all values of $n_{Si/Al}(i)$ is the total number of Brønsted acid sites per unit mass of the zeolite, $N_{Si/Al}$.

SCHEME 1: Illustration of Products Formed by the Cracking of C_3-C_6 Alkanes

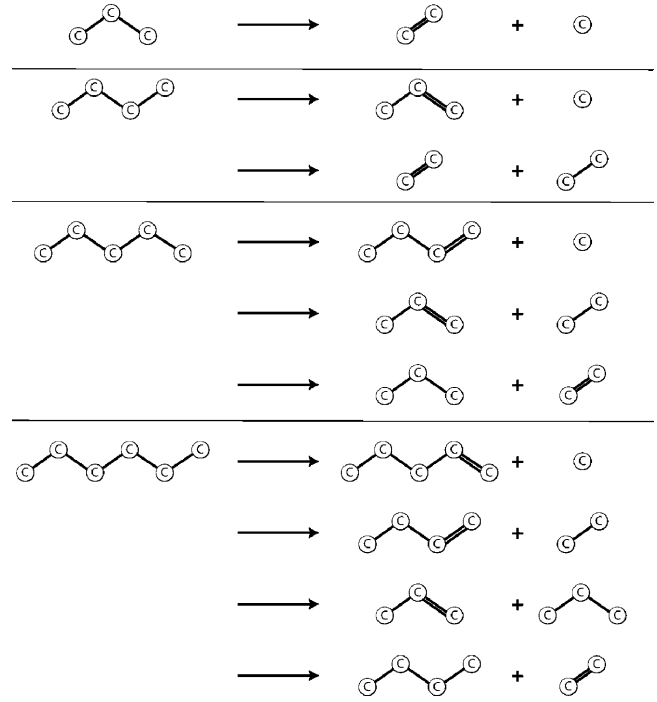

The reaction rate of reaction *j* per unit zeolite mass occurring at acid sites of type *i* is given, therefore, by

$$r(i,j,P_A,n_{Si/Al}(i)) = k_{int}(i,j)\langle N_{react}(i,j,P_A,n_{Si/Al}(i))\rangle \quad (1)$$

The overall reaction rate involves summation over *I* different types of acid sites and *J* reactions paths

$$r(P_A,N_{Si/Al}) = \sum_{j}^{J}\sum_{i}^{I} k_{int}(i,j)\langle N_{react}(i,j,P_A,n_{Si/Al}(i))\rangle \quad (2)$$

Equations 1 and 2 are applicable for arbitrary alkane partial pressures and Si/Al ratios. As discussed below, the intrinsic rate coefficient can be obtained from quantum chemical calculations and the number of molecules in the reactant state can be obtained from a Monte Carlo simulation.

Experimental studies of alkane cracking are carried out at high temperatures and moderate alkane pressure for which a number of alkane molecules adsorbed per unit zeolite mass, $\langle N_{ads}(P_A,N_{Si/Al})\rangle$, is in the Henry regime. In this case, the number of adsorbed molecules in the zeolite can be obtained from the Henry coefficient, K_H

$$\langle N_{ads}(P_A,N_{Si/Al})\rangle = K_H(N_{Si/Al})P_A \quad (3)$$

The dependence of K_H on the Si/Al ratio expresses the fact that the Henry's constant can depend on the density of acid sites in the zeolite. In the Henry regime interactions between the molecules can be ignored and, hence, the probability of finding a molecule in the reactant state (i,j), $P_{react}(i, j, n_{Si/Al}(i))$, is independent of alkane loading. Therefore, we can write for the number of molecules in the reactant state

$$\langle N_{react}(P_A, N_{Si/Al})\rangle = P_{react}(i,j,n_{Si/Al}(i))K_H(N_{Si/Al})P_A \quad (4)$$

From a computational point of view this expression has as practical advantage in that both the Henry coefficient and the probability of a molecule being in the reactant state can be obtained from an NVT simulation at infinite dilution (i.e., one molecule per unit mass of zeolite).

For the purposes of the present analysis we also consider that the alkane molecules are sufficiently short that each one interacts with only one active site at a time. As a consequence, we can define a probability per type of acid site

$$p_{react}(i,j) = \frac{P_{react}(i,j,n_{Si/Al}(i))}{n_{Si/Al}(i)} \quad (5)$$

Substitution of eq 5 into eq 4 gives

$$\langle N_{react}(P_A, N_{Si/Al})\rangle = p_{react}(i,j)n_{Si/Al}(i)K_H(N_{Si/Al})P_A \quad (6)$$

Using this equation to compute the overall reaction rate we obtain

$$r(P_A, N_{Si/Al}) = \sum_j^J \sum_i^I k_{int}(i,j)p_{react}(i,j)n_{Si/Al}(i)K_H(N_{Si/Al})P_A \quad (7)$$

As discussed below, we further assume that the intrinsic reaction rate is similar for all acid sites, that is, $k_{int}(i,j) = k_{int}(j)$, which then allows eq 7 to be rewritten as

$$r(P_A, N_{Si/Al}) = \sum_j^J k_{int}(j) \sum_i^I p_{react}(i,j)n_{Si/Al}(i)K_H(N_{Si/Al})P_A \quad (8)$$

The apparent, first-order rate coefficient for cracking of an alkane is now defined as

$$k_{app} = \frac{\sum_j^J k_{int}(j) \sum_i^I p_{react}(i,j)n_{Si/Al}(i)K_H(N_{Si/Al})}{\sum_i^I n_{Si/Al}(i)} \quad (9)$$

This expression can be further simplified by defining the average value of $p_{react}(i,j)$, $\langle p_{react}(j)\rangle$, as

$$\langle p_{react}(j)\rangle = \frac{\sum_i^I p_{react}(i,j)n_{Si/Al}(i)}{\sum_i^I n_{Si/Al}(i)} \quad (10)$$

Introducing eq 10 into eq 9 allows us to write

$$k_{app} = \sum_j^J k_{int}(j)\langle p_{react}(j)\rangle K_H(N_{Si/Al}) \quad (11)$$

Intrinsic Reaction Rates. As noted in the preceding section, the rate coefficient for reaction j is specific for acid site i. Since the computation of all values of $k_{int}(i,j)$ from first principles is computationally very demanding, we assumed that a reasonable estimate of the reaction rate could be obtained by considering a representative Brønsted acid center in MFI and FAU. We further assumed that the rate coefficients $k_{int}(j)$ calculated in this manner provided a reasonable approximation of the rate coefficients at other sites in both zeolites.

The rate coefficients, $k_{int}(j)$, were determined for the cracking of specific C−C bonds in C_3−C_6 alkanes in MFI and FAU. For both zeolites the Brønsted-acid center and a portion of the zeolite framework were represented by a cluster containing five T-sites. The use of such small clusters is attractive from the perspective of computational cost; however, recent work has shown that small clusters do not give an accurate representation of molecular heats of adsorption and activation energies for elementary reactions.[31−33] To assess the importance of system size, we carried out a limited series of calculations using a T23 cluster of MFI, as well as plane-wave DFT calculations for the entire H-ZSM-5 unit cell to determine the activation energies for C−C bond cleavage occurring during the cracking of propane and butane.

For the T5 cluster representation of MFI, all Si atoms were placed initially at their crystallographic positions, as reported by Olson et al.[34] The location of Al in the zeolite framework is difficult to define. Both experimental[35] and theoretical[36] studies aimed at determining the preferential locations for Al substitution into MFI do not lead to a definitive conclusion because the differences in the energies associated with replacement of a Si by Al at different T sites are small. Thus, the location of Al atoms in the zeolite framework is controlled more by the kinetics of zeolite synthesis than by thermodynamics. Nevertheless, there is some evidence that Al siting is not random and that in MFI the T12 site is preferred.[35,37] On the basis of these findings and other theoretical studies on H-MFI[38−40] we selected the T12 position as a representative T site for all Al substitution (see Figure S.4 in the Supporting Information). The terminal Si−O bonds of the cluster were replaced by Si−H bonds oriented in the direction of the former Si−O bond. The Si−H bond length was set to 1.487 Å, which is the optimized bond length for SiH_4 at the B3LYP/TZVP level of theory. The resulting coordinates for the terminal H atoms along with the coordinates for the Si atoms were held fixed throughout all subsequent calculations. In the case of the T23 cluster, the Al atom was again placed at the T12 site and the cluster was terminated in the same manner as the T5 cluster, except that only the terminating H-atoms were held fixed during the optimization. The T5 cluster representation of FAU is based on the crystallographic positions for dehydrated NaX.[41] In FAU, sodalite units are connected by double six-membered rings

arranged in 1.2 nm wide supercages accessible through 0.72 nm windows. In contrast to MFI, all tetrahedral atom positions are equivalent. However, adsorption of alkanes tends to be limited to the supercages. Therefore we paid attention that the bridging hydroxyl group was directed into the free space of the supercages. The cluster was terminated in the same manner as the T5 cluster representing MFI.

Quantum chemical calculations were performed with the TURBOMOLE V5.10 suite of programs[42] in C1 symmetry using gradient-corrected density functional theory (DFT). To represent the effects of exchange and correlation, Becke's three-parameter exchange functional[43] and the correlation functional of Lee, Yang, and Parr (B3LYP)[44] were used with very fine numerical grid size (m5).[45] Basis sets at the double-ζ level with polarization functions (SV(P))[46] were used for all atoms during optimizations. This moderate basis set size was justified by optimizing the reactant and transition state structure for the cracking of propane using a basis set of triple-ζ quality (TZVP).[47] The activation energy obtained with the TZVP basis set was higher than the one obtained with the SV(P) basis set by only 4.4 kJ/mol leading us to conclude that the SV(P) basis set offers a good compromise between accuracy and computational efficiency. For selected structures additional single point energy calculations have been performed with a basis set of quadruple-ζ quality (QZVP).[48] In the minimum energy structure optimizations, energies were converged to 10^{-8} Ha and the maximum norm of the Cartesian gradient was converged to 10^{-5} Ha/bohr. Transition states were localized using a combination of interpolation and local methods. The growing-string method[49] was used in mass-weighted coordinates with a maximum of 13 to 16 nodes. After the two ends of the growing string joined, the growing-string method was terminated and an approximate saddle point was identified. The PRFO method[50] was employed to refine the position of the saddle point. A gradient-norm convergence criterion of 5×10^{-4} Ha/bohr was used for the transition-state searches. To confirm that the transition states were connected to the correct energy minima, each transition state was perturbed slightly along the reaction coordinate in the reactant and product directions. The perturbed geometries were then used as starting points for energy minimization. In most cases the desired energy minimum was obtained directly. In some cases mechanistically irrelevant barriers of less than 2 kJ/mol associated with small structural rearrangements of the adsorbate had to be surmounted to reach the desired energy minimum.

Recent studies have shown that the B3LYP functional does not capture the effects of dispersive forces very accurately.[51,52] Since such forces could affect the results of our study, we carried out a limited series of calculations using the M05-2X functional,[53] which has been demonstrated to describe the effects of dispersive forces.[51,54] These calculations were carried out with the Gaussian suite of programs[55] using 6-31G* and 6-311+G(2df, 2p)[56,57] basis sets to assess the effects of the basis set size, in addition to the choice of functional, on the values of the activation energies for C−C bond cleavage. Activation energies were determined for each of the reaction channels considered for propane through hexane (see Scheme 1) using the T5 cluster and for the cracking of propane and butane using the T23 cluster. Additional MP2 single-point energy calculations employing Ahlrichs' improved triple-ζ basis set (def2-TZVPP)[58] were conducted to assess how this higher level of theory compares with calculations done at the DFT/M05-2X/6-311+G(2df, 2p) level. We used the parallelized version of TURBOMOLE "ricc2"-module[59,60] and employed the resolution of the identity (RI) approximation[61−63] with optimized auxiliary basis sets[64] in combination with a frozen-core ansatz. Electrons in molecular orbitals corresponding to C 1s, O 1s, Al 1s, and Si 1s atomic orbitals were excluded from the MP2 correlation scheme. Moreover, for propane and butane cracking we performed DFT calculations applying periodic boundary conditions using the Vienna ab initio simulation package (VASP).[65−68] The purpose of these calculations was to investigate further the influence of the system size on the barrier heights for alkane cracking. The computational details are reported in the Supporting Information.

Intrinsic rate coefficients are calculated from conventional transition state theory[69−71]

$$k(T) = \frac{k_B T}{h} \frac{Q_{TS}(T)}{Q_R(T)} \exp[-E^{\ddagger}/RT] \tag{12}$$

where k_B is Boltzmann's constant, h is Planck's constant, T is the absolute temperature, and $E^{\ddagger}$ is the difference in electronic energies between the transition state and the reactant state. With Q_{TS} and Q_R, we denote the partition functions of the transition state and the reactant state, respectively. For the calculation of the partition functions, we used the harmonic approximation and assumed that adsorbate and transition state are rigid in space and have only vibrational degrees of freedom.

Henry Coefficient and Probabilities of Alkanes Being in the Reactant State. Both the Henry coefficient and the probability to finding alkanes in the reactant state (i,j) were determined using configurational-bias Monte Carlo (CBMC) in the NVT-ensemble. It was assumed that the zeolite framework is purely siliceous with all atoms held in their crystallographic positions. The interactions of a single adsorbate molecule with the zeolite framework were modeled with a Lennard-Jones-type potential using the force field parameters of Dubbeldam et al.[1] Alkane molecules were treated with CH_3 and CH_2 groups being represented as united atoms connected by harmonic bonds. Bond bending, torsion, and internal van der Waals interactions were also included. Additional information about the model can be found in the Supporting Information.

To enhance computational efficiency, adsorbate-framework interaction energies were determined from precalculated interpolation grids for each pseudoatom type. Our MC scheme included translation, rotation, and partial and full molecule regrowth. All of the thermodynamic properties reported here were obtained from simulations consisting of at least 500 000 Monte Carlo cycles. At the experimental conditions of interest, the system is in the Henry regime, which implies that all calculations can be carried out at the limit of zero loading. Below we summarize the equations we have used, and a more complete discussion of the methods used can be found elsewhere.[1]

The Henry's law constant was calculated from the CBMC simulations, using the ratio of the average Rosenbluth weights of the adsorbate in the zeolite, $\langle W \rangle$, and in an ideal gas phase, $\langle W_{ig} \rangle$, respectively.

$$K_H = \frac{1}{\rho_f RT} \frac{\langle W \rangle}{\langle W_{ig} \rangle} \tag{13}$$

where ρ_f is the mass density of the zeolite framework.

To further analyze the thermodynamics of adsorption, we also computed the enthalpy and free energy of adsorption. The enthalpy of adsorption, ΔH_{ads}, can be obtained from

$$\Delta H_{ads} = \Delta U_{ads} - RT = \langle U_{hg} \rangle - \langle U_h \rangle - \langle U_g \rangle - RT \quad (14)$$

in which $\langle U_{hg} \rangle$, $\langle U_h \rangle$, and $\langle U_g \rangle$ are the internal energy of the zeolite-adsorbate system, the zeolite, and the gas, respectively. The internal energy of the zeolite is identically zero because the framework atoms are maintained in a fixed arrangement.

In the Henry's regime, the Gibbs free energy for alkane adsorption into the zeolite, is related to the Henry's constant by the expression

$$\Delta G_{ads} = -RT(1 + \ln(\rho_f RTK_H)) \quad (15)$$

where ρ_f is the mass density of the framework. The entropy of adsorption, ΔS_{ads}, can then be calculated from the free energy and enthalpy of adsorption, as shown below

$$\Delta S_{ads} = \frac{\Delta H_{ads} - \Delta G_{ads}}{T} \quad (16)$$

To understand how the probability of an alkane molecule being in the reacting state, $P_{react}(i,j)$, is determined, it is useful to first consider the potential energy diagram shown in Figure 1. Upon adsorption from the gas phase into a zeolite, an alkane molecule experiences a decrease in potential of about 40−60 kJ/mol, depending on the number of carbon atoms in the alkane. An additional reduction in potential energy occurs when an adsorbed alkane molecule associates with a Brønsted acid site. As discussed below and determined experimentally, this change in potential is small, typically 10 kJ/mol.[72,73] The activation barrier for cracking is then the distance from the bottom of the well for alkane association with the acid site to the top of the transition state. Because the energy of association of an alkane with a Brønsted-acid site is small at temperature where cracking occurs (>773 K) only a small fraction of the molecules adsorbed within the zeolite will be in the reactant state (i,j). In prior analyses of zeolite-catalyzed cracking of alkanes, $P_{react}(i,j)$ was assumed implicitly to be 1.0,[29] which meant that all adsorbed molecules are equally likely to be available for reaction. However, careful consideration of the finite size of alkanes and the size of the spaces in which Brønsted-acid sites occur suggests that this is generally not the case. For an alkane to crack via pathway j, the C−C bond that undergoes cleavage for that pathway must be within 2.5−3.5 Å of the oxygen atom associated with the Brønsted-acid site. However, a complication arises in defining which of the four O atoms associated with a given Al T site is the one on which the proton resides, since at the temperatures where cracking occurs, the protons hop rapidly between the four O atoms.[39] As this hopping rate is much faster than the rate of cracking, the reactant state needs to be extended to each of the O atoms connected directly to the Al. Simple geometric arguments show that the reactant volume defined by these four spheres around the oxygen atoms is equivalent to a sphere of radius 5.0 Å centered on the Al atom (see Supporting Information).

The values $P_{react}(i,j)$ were determined in the following manner. After each 10 MC steps the number of C−C bonds associated with reaction j present within a 5.0 Å radius from T site type i are counted, and once all MC steps have been completed, the accumulated sum for each type of T site in a unit cell of the zeolite is divided by the total number of MC points accumulated in the zeolite unit cell. The basis for choosing the cutoff radius as 5 Å and the influence of the choice of cutoff radius on the magnitude of $P_{react}(i,j)$ are discussed in the Supporting Information. A point to be noted is that while the quantum calculations give a specific configuration of the alkane adsorbed at the Brønsted-acid site, that is, the lowest energy configuration at 0 K, it is not required that this configuration be reproduced in the sampling of configurations used to determine $p_{react}(i,j)$. Thus, all configurations satisfying the condition that the C−C bond of an alkane to be cracked via pathway j lie within a 5.0 Å radius of the Al atom associated with a proton are counted. Examples of the $P_{react}(i,j)$ for different alkane zeolite systems are given in the Supporting Information.

The computed values of $P_{react}(i,j)$ are then used to determine the corresponding values of $p_{react}(i,j)$. The value of $p_{react}(i,j)$ is determined by dividing $P_{react}(i,j)$ by the concentration of sites of type i per unit zeolite mass $n_{Si/Al}(i)$, in accordance with eq 5. The value of $\langle p_{react}(j) \rangle$ is determined from eq 10.

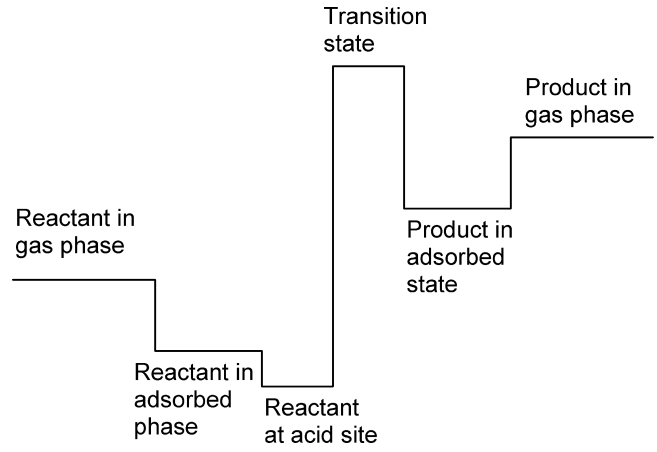

Figure 1. Schematic of potential energy diagram for alkane cracking.

TABLE 1: Values of ΔH_{int}, ΔS_{int}, and Total k_{int} for the Cracking of C_3−C_6 Alkanes on MFI Calculated from DFT and Absolute Rate Theory for 773 K

molecule	ΔH_{int} kJ/mol	ΔS_{int} J/(mol K)	$k_{int}/10^{-4}$ 1/s	j	products	
propane	216.5	−34.9	5.40	1	CH_4	C_2H_4
n-butane	210.5	−36.7	11.70	1	CH_4	C_3H_6
	192.7	−53.2	25.9	2	C_2H_6	C_2H_4
n-pentane	212.8	−38.7	6.40	1	CH4	1-C_4H_8
	190.3	−54.0	33.9	2	C_2H_6	C_3H_6
	190.9	−50.6	46.2	3	C_3H_8	C_2H_4
n-hexane	208.5	−43.3	7.1	1	CH_4	1-C_5H_{10}
	190.0	−52.7	41.7	2	C_2H_6	1-C_4H_8
	190.1	−57.4	23.1	3	C_3H_8	C_3H_6
	189.8	−46.8	86.4	4	C_4H_{10}	C_2H_4

Results and Discussion

Intrinsic Rate Coefficient for Alkane Cracking. Table 1 lists the enthalpy and entropy of activation for the cracking of each alkane on MFI. Multiple entries are given for a given alkane when there are more than one set of products that can be formed (see Scheme 1). All of the calculations presented are based on energies and vibrational frequencies determined using the T5 cluster and DFT/B3LYP/SV(P) level of theory. In general, the activation enthalpy tends to decrease with increasing chain length. This may reflect the increased stability of transition states with longer chains that can donate more electron density to stabilize the carbocation. The calculated activation entropies are always negative but do not show a clear trend in magnitude and appear to depend more on the specific

TABLE 2: Values of ΔH_{int}, ΔS_{int}, and Total k_{int} for the Cracking of C_3-C_6 Alkanes on FAU Calculated from DFT and Absolute Rate Theory for 773 K

molecule	ΔH_{int} kJ/mol	ΔS_{int} J/(mol K)	$k_{int}/10^{-4}$1/s	j	products	
propane	237.0	−34.4	0.25	1	CH_4	C_2H_4
n-butane	227.6	−45.1	0.30	1	CH_4	C_3H_6
	199.9	−56.7	5.45	2	C_2H_6	C_2H_4
n-pentane	226.3	−44.4	0.39	1	CH_4	1-C_4H_8
	195.7	−55.2	12.5	2	C_2H_6	C_3H_6
	201.6	−44.3	18.6	3	C_3H_8	C_2H_4
n-hexane	225.9	−44.5	0.41	1	CH_4	1-C_5H_{10}
	194.8	−58.3	9.9	2	C_2H_6	1-C_4H_8
	197.6	−46.1	28.0	3	C_3H_8	C_3H_6
	200.6	−45.7	18.4	4	C_4H_{10}	C_2H_4

transition state than the composition of the reacting alkane. These conclusions differ from those reported by Bhan et al.[30] In this study, the authors determined the intrinsic activation enthalpy and entropies from the experimentally observed apparent kinetic parameters and an extrapolation of the adsorption constants measured at 298 K to the temperature at which cracking occurred, 773 K. On the basis of their approach the authors conclude that the intrinsic activation enthalpy is virtually constant with respect to chain length and that the intrinsic activation entropy increases monotonically to a significant degree (become more positive) proceeding from propane to *n*-hexane.

Table 2 lists results similar to those shown in Table 1 but for alkane cracking on FAU, determined using the T5 cluster and DFT/B3LYP/SV(P) level of theory. It is noted that the activation enthalpies for each elementary reaction are higher than those found for MFI, reflecting the lower acidity of FAU relative to MFI. It is notable, though, that with only limited exceptions, the activation energies for alkane cracking on FAU are similar to those on MFI. Likewise, the trend in activation energy with alkane carbon number is similar to that seen for MFI. Comparison of the rate coefficients predicted for MFI and FAU using the same cluster size and level of theory reveals that the rate coefficients for each reaction channel are noticeably lower for FAU than MFI, consistent with what has been suggested by Bhan et al.[30] and reported recently by Katada et al.[74]

To assess the effects of the functional and basis set used for the calculation of activation energies, additional calculations were done at the DFT/M05-2X/6-31G*, DFT/M05-2X/6-311+G(2df,2p), and MP2/def2-TZVPP levels. The activation energies obtained at these levels are shown in Table 3 and compared with those obtained at the DFT/B3LYP/SV(P) level. In considering these results, it should be recognized that the 6-31G* basis set is similar to the SV(P) used in TURBOMOLE. Comparison of the activation barriers from DFT/B3LYP/SV(P) and DFT/M05-2X/6-31G* calculations shows that using the M05-2X functional increases the activation barrier for propane cracking to methane and ethene, and the activation barrier for cracking of butane to methane and propene by about 16 kJ/mol, but gives activation barriers that are roughly the same (within <5 kJ/mol) for the remaining elementary reactions. Increasing the quality of the basis set to 6-311+G(2df,2p) using the M05-2X functional has little effect on the activation barriers for propane cracking to methane and ethene or for butane cracking to methane and propene, but decreases the activation barriers for all other processes by about 7−10 kJ/mol. Table 3 shows that raising the level of theory further to MP2/def2-TZVPP has either no effect on the activation energies calculated at the DFT/M05-2X/6-311+G(2df,2p) level or increases them by 12 kJ/mol or less.

The effects of cluster size on the activation barriers for propane and butane cracking are shown in Table 4 for various levels of theory. It is seen that increasing cluster size from T5 to T23 at a given level of theory decreases the activation barrier for cracking of propane by 34−70 kJ/mol and for cracking of butane into methane and propene by 24−60 kJ/mol, the deviation growing in general with increasing level of theory. However, for cracking of butane into ethane and ethene the decrease of the barrier heights is smaller (6 kJ/mol), suggesting that significant system size dependence is only observed for cracking of the α-bonds. It is also evident that increasing the level of theory used with the T23 cluster decreases the activation barrier relative to that determined with DFT/B3LYP/SV(P); however this decrease is less than 12 kJ/mol.

The results presented in Tables 3 and 4 clearly demonstrate that size of the cluster used to perform the quantum calculations and the level of theory affect the activation barrier determined.

TABLE 3: Activation Energies from Different Methods. The Underlying Geometry Is the MFI-T5 Cluster Optimized at the B3LYP/SV(P) Level of Theory

	DFT results			MP2 results		
molecule	B3LYP/SV(P)	M05-2X/6-31G*	M05-2X/6-311+G(2df,2p)	def2-TZVPP		
propane	234.6	251.5	251.4	263.5	CH_4	C_2H_4
n-butane	228.5	245.5	245.8	257.8	CH_4	C_3H_6
	206.5	206.2	197.9	199.2	C_2H_6	C_2H_4
n-pentane	225.3	224.1	213.6	219.8	CH_4	1-C_4H_8
	204.8	201.9	193.4	194.2	C_2H_6	C_3H_6
	204.2	200.6	190.6	192.1	C_3H_8	C_2H_4
n-hexane	221.6	223.4	213.0	220.2	CH_4	1-C_5H_{10}
	204.6	201.4	192.5	193.0	C_2H_6	1-C_4H_8
	204.4	198.9	191.1	191.2	C_3H_8	C_3H_6
	202.6	199.2	188.7	190.4	C_4H_{10}	C_2H_4

TABLE 4: Activation Energies from Different Methods Obtained on the T23 Cluster for Propane and Butane Cracking[a]

	DFT results			MP2 results		
molecule	B3LYP/SV(P)	M05-2X/6-31G*	M05-2X/6-311+G(2df,2p)	def2-TZVPP		
propane	201.7	191.8	188.2	192.3	CH_4	C_2H_4
n-butane	204.1	194.2	191.2	196.6	CH_4	C_3H_6
	200.2	186.8	183.2	188.5	C_2H_6	C_2H_4

[a] The underlying geometry is the MFI-T23 cluster optimized with B3LYP/SV(P).

TABLE 5: Plane-Wave DFT (PBE) Results for Intrinsic Energy Barriers, Intrinsic Enthalpy Barriers (773 K), and Intrinsic Activation Entropies (773 K)

molecule	E kJ/mol	ΔH_{int} kJ/mol	ΔS_{int} J/(mol K)	j	products
propane	172.8	156.2	−68.1	1	CH_4 C_2H_4
n-butane	172.9	156.4	−70.9	1	CH_4 C_3H_6

TABLE 6: Values of ΔH_{ads} and ΔS_{ads} Calculated from CBMC and Experiments[a]

	T	ΔH_{ads} (CBMC)	ΔS_{ads} (CMBC)	ΔH_{ads} (experiment)
	K	kJ/mol	J/(mol K)	kJ/mol
MFI				
propane	573	−37.8	−41.1	−40[(1)]
	773	−37.8	−38.6	
n-butane	573	−46.2	−50.9	−49[(1)]
	773	−45.9	−47.8	
n-pentane	573	−55.8	−62.2	−57.7[(2)] (137)
	773	−54.8	−58.2	
n-hexane	573	−65.3	−73	−68.8[(2)] (137)
	773	−64.2	−69.0	
FAU				
propane	573	−21.4	−19.6	
	773	−21.5	−17.2	
n-butane	573	−23.6	−20.1	
	773	−24.6	−19.1	
n-pentane	573	−27.5	−23.2	−40.4[(2)] (30)
	773	−28.3	−21.8	
n-hexane	573	−31.4	−26.3	−47.7[(2)] (30)
	773	−32.0	−24.8	

[a] Data from (1) Sun et al.[77] and (2) Denayer et al.[76] Experimental Si/Al ratios are given in parentheses.

Increasing the cluster size leads to a significant reduction in the activation barrier, consistent with the recent findings of Hansen et al.[31] for benzene alkylation by ethene. Improving the level of theory results in smaller changes in the activation barrier, which may be positive or negative depending on the specifics of the reaction considered and the size of the cluster. To further evaluate our cluster results we have calculated energy barriers for propane and butane cracking using plane-wave DFT. The results are presented in Table 5. Both reactions have a barrier height of 173 kJ/mol. However, it is well-known that PBE tends to underestimate barrier heights.[75] For the alkylation of benzene it has been shown recently that this underestimation can be as large as 30 ± 10 kJ/mol.[31] As a result, our barriers calculated on the T5 cluster are reasonable approximations although an uncertainty of at least ±10 kJ/mol will be present. Since the calculation of all reaction pathways considered in this study using a T23 cluster at the highest level of theory or periodic DFT is prohibitively expensive, calculations of the apparent rate coefficient were carried out using the intrinsic rate coefficients determined using the T5 cluster at the DFT/B3LYP/SV(P) level. The consequence of this choice is discussed below in the context of comparisons of the theoretically determined apparent rate coefficient and its comparison with experimental data. The impact of using a larger cluster and higher level of theory are discussed there as well.

Adsorption Thermodynamics. Table 6 compares calculated values for the enthalpy of adsorption with experimental values reported by Denayer et al.[76] and Sun et al.[77] for light alkanes adsorbed on the same zeolites. Our calculated values capture the expected decrease in adsorption enthalpy with increasing n-alkane chain length. The enthalpy of adsorption is dominated by the dispersive interactions between the alkane and the pore walls.[72] Narrower pore zeolites tended to have more negative adsorption enthalpies and a stronger dependence of adsorption enthalpy on chain length, a result of stronger dispersive interactions. Table 6 also shows that the adsorption enthalpy for each alkane is essentially constant with respect to temperature for the temperatures relevant to monomolecular cracking. All experimental enthalpies are higher in magnitude than the corresponding calculated value, as is to be expected since Denayer et al.[76] used the acid form of the zeolite.

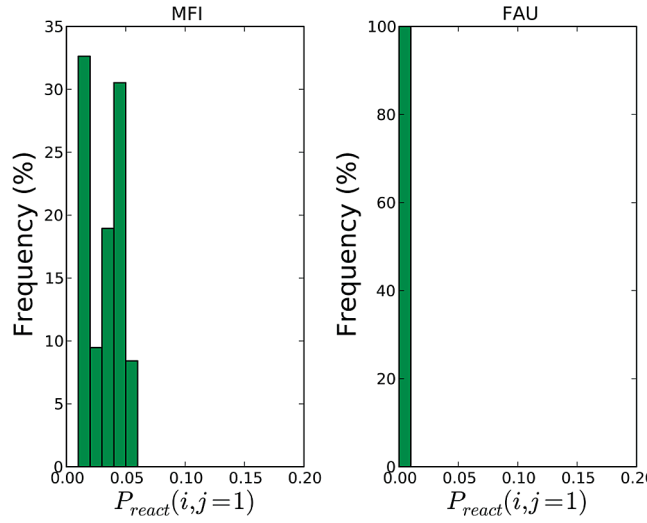

Figure 2. Distribution of values of $P_{react}(i,j = 1)$ for the cracking of butane at the terminal C−C bond on MFI and FAU.

Adsorption entropies, calculated using eq 16, are also reported in Table 6. The entropy change upon adsorption follows the expected trend, becoming more negative with increasing chain length and smaller zeolite pore size. The chain length dependence reflects the greater loss of configurational freedom that larger molecules experience. Narrower pores restrict molecular moves more than larger pores, leading to more negative adsorption entropies for MFI compared to FAU.

Probability of Being in the Reactant State, $P_{react}(i,j)$. As noted above $P_{react}(i,j)$ represents the probability that the C−C alkane molecule is in the reactant state for reaction j to occur on a Brønsted-acid site associated with Al in T site type i. It is, therefore, expected that the value of $P_{react}(i,j)$ for a given alkane undergoing reaction j will differ from one zeolite to another. This point is well illustrated for the cracking of the terminal C−C bond in butane ($j = 1$), which produces methane and propene. Figure 2 shows a histogram of values for $P_{react}(i,j)$ for this reaction catalyzed by MFI and FAU. For ease of comparison, the heights of the peaks in the histograms are normalized so that the sum of all peaks is unity. We note for that FAU, which has only a single T-site symmetry, there is essentially one value of $P_{react}(i,j)$. As the number of crystallographically distinct T-sites increases, the number of peaks increases; thus, the largest number of peaks is seen for MFI, which has 12 T-site types. All calculated values of $\langle p_{react}(j)\rangle$ are listed in Table 7. Temperature also affects the value of $P_{react}(i,j)$. Figure 3 shows that the probability of finding an adsorbate in the reactant state decreases with increasing temperature. This effect influences the apparent activation energy, as discussed below.

Apparent Rate Coefficients for Alkane Cracking. To assess the quality of our theoretical approach, we compared the apparent rate coefficients that we predicted with those reported by Narbeshuber et al.[25] for the cracking of C_3−C_6 n-alkanes on MFI with Si/Al = 35. These authors differentiated between cracking rates and dehydrogenation rates by careful deconvolution of the product distributions. Since the majority of the

TABLE 7: Values of k_{int}, K_H, $\langle p_{react}(j)\rangle$, and k_{app} for Alkane Cracking on MFI and FAU Calculated for $T = 773$ K

	$k_{int}/10^{-4}$ s^{-1}				K_H mol kg^{-1} bar^{-1}	$\langle p_{react}(j)\rangle$ kg (mole sites)$^{-1}$				$k_{app}/10^{-3}$ mol (mol sites)$^{-1}$ s^{-1} bar^{-1}
	j 1	2	3	4		j 1	2	3	4	
MFI										
propane	5.4				3.5	0.36				0.68
n-butane	11.7	25.9			4.0	0.37	0.16			3.4
n-pentane	6.4	33.9	46.2		4.6	0.42	0.36	0.36		6.7
n-hexane	7.1	41.7	23.1	46.2	5.5	0.44	0.39	0.19	0.39	32
FAU										
propane	0.25				3.6	0.1				0.009
n-butane	0.30	5.45			4.6	0.08	0.03			0.0086
n-pentane	0.39	12.5	18.6		5.9	0.08	0.05	0.05		0.94
n-hexane	0.41	9.9	28.0	18.4	7.4	0.09	0.05	0.02	0.05	1.5

acid site in MFI with Si/Al = 35 are isolated, this system provides an ideal case for testing our theoretical approach. It should also be noted that the narrow pore size of the MFI framework disfavors the bimolecular cracking pathway.[16] The values of k_{app} reported by Narbeshuber et al. are compared in Figure 4 with those determined using the calculated values of Values of k_{int}, K_H, and $\langle p_{react}(j)\rangle$ listed in Table 7 and eq 11. It is evident that while the predicted values of k_{app} follow the trend with increasing carbon number seen experimentally, the predicted values of k_{app} are a factor of 10 (propane) to 50 (hexane) lower than those observed. We believe that the major source of the discrepancy is the accuracy of our determination of the

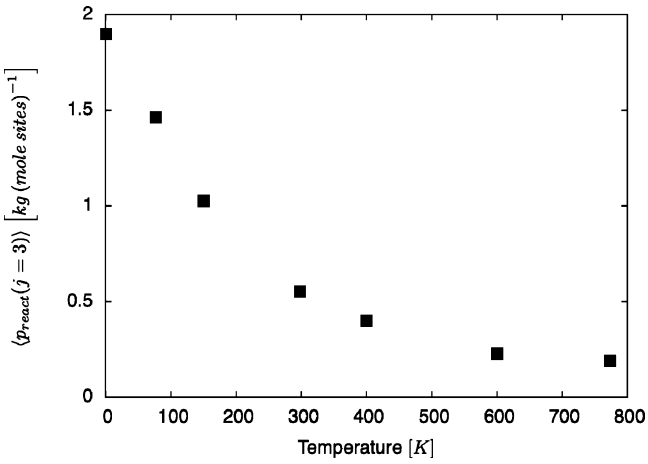

Figure 3. Effect of temperature on the value of $\langle p_{react}(j = 3)\rangle$ for the cracking of *n*-hexane at the center C−C bonds on MFI.

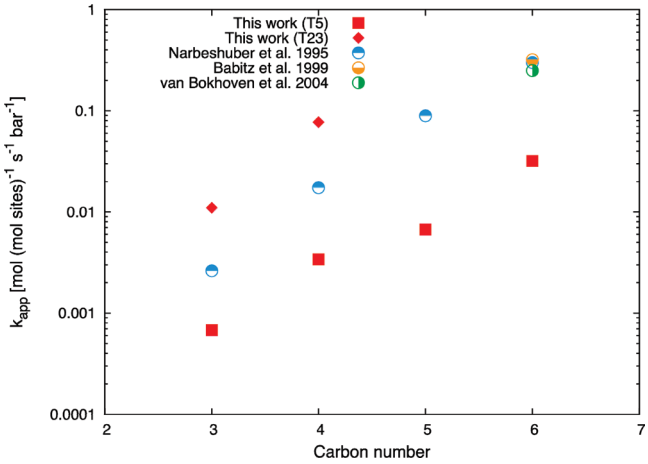

Figure 4. Comparison of calculated and experimental values of k_{app} for the cracking of n-alkanes on MFI at 773 K. Experimental data taken from van Bokhoven et al.,[27] Babitz et al.,[19] and Narbeshuber et al.[25]

TABLE 8: Values of ΔH_{int}, ΔS_{int}, and k_{int} Determined for the T23 Clusters at the DFT/B3LYP/SV(P) Level

molecule	ΔH_{int} kJ/mol	ΔS_{int} J/(mol K)	$k_{int}/10^{-4}$ 1/s	j	products
propane	186.2	−51.3	87.4	1	CH_4 C_2H_4
n-butane	187.7	−42.4	205.0	1	CH_4 C_3H_6
	183.5	−37.1	733.5	2	C_2H_6 C_2H_4

TABLE 9: Apparent Activation Energies for Propane and Hexane Cracking on MFI[a]

	calculated values (kJ/mol)		
molecule	T5 cluster	T23 cluster	observed values (kJ/mol)
propane	179	148	147[(1)], 155[(4)]
butane	152	138	135[(4)]
pentane	138		120[(4)]
hexane	127		111 ± 9.6[(2)] 149[(3)] 105[(4)]

[a] Experimental data taken from (1) Xu et al.,[29] (2) van Bokhoven et al.,[27] (3) Babitz et al.,[19] and (4) Narbeshuber et al.[25] The experimental values for MFI from van Bokhoven et al.[27] were taken as an average over samples with different Si/Al ratios.

intrinsic rate coefficient for C−C bond cleavage, k_{int}. As discussed above, the largest source of error in these calculations is the use of a small (T5) cluster. To assess the effect of cluster size, values of k_{int} were determined using the T23 cluster at the DFT/B3LYP/SV(P) level of theory. The results of these calculations are presented in Table 8 for propane and butane cracking and compared with the values determined using the T5 cluster at the same level of theory. In the case of propane, the value of k_{int} is 16.4 times higher when the T23 cluster is used. For butane the factors are 17.5 and 28.3, respectively. Values of k_{app} were calculated for propane and butane cracking using the values of k_{int} given in Table 8. As seen in Figure 4 values of k_{app} now exceed those observed experimentally by about a factor of three to four.

Table 9 compares the apparent activation energies determined for propane and hexane cracking using the T5 and T23 clusters and compares the values obtained with those observed experimentally. For propane, the apparent activation energy determined using the T5 cluster is 179 kJ/mol and decreases to 148 kJ/mol for the T23 cluster, a value that is in excellent agreement with the experimentally observed values, 147 and 155 kJ/mol. Similarly good agreement is observed for butane cracking. The value of the apparent activation energy is 138 kJ/mol determined using the T23 cluster, which compares very favorably with the experimental value of 135 kJ/mol. Here too, the apparent activation energy calculated using the T5 cluster yields a value that is too large, 152 kJ/mol. In the case of pentane and hexane, the apparent activation energy determined using the T5 cluster are 138 and 127 kJ/mol, respectively, whereas the experimental values are 120 kJ/mol for pentane and 111 ± 9.6 kJ/mol, 149

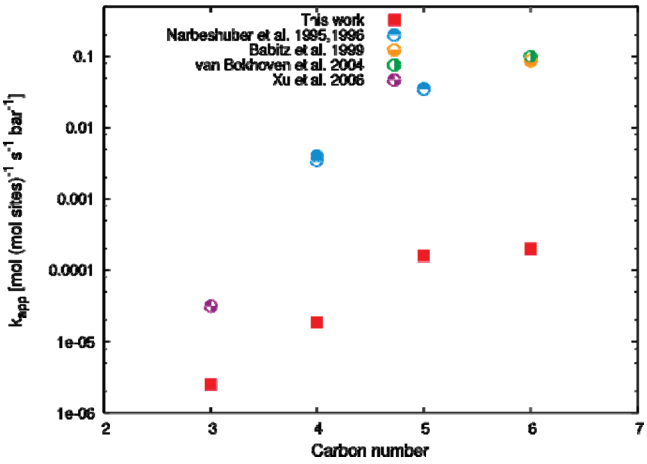

Figure 5. Comparison of the calculated and experimental values of k_{app} for the cracking of of n-alkanes on FAU at 773 K. Experimental data taken from van Bokhoven et al.,[27] Babitz et al.,[19] Narbeshuber et al.,[25,73] and Xu et al.[29] The value of k_{app} from Xu et al. is extrapolated from k_{app} and E_a measured for 823 K.

kJ/mol, and 105 kJ/mol for hexane, as reported by different investigators. While values of the apparent activation energy for pentane and hexane cracking was not carried out using the T23 cluster, such calculations would be expected to yield a value closer to the experimentally observed values based on the evidence presented for propane and butane cracking. Table 9 also demonstrates that the theoretically determined value for the apparent activation energy falls monotonically with increasing carbon number of the alkane, consistent with what is observed experimentally.

As a further evaluation of our simulation approach, we compared the values of k_{app} predicted for the cracking of butane, pentane, and hexane on FAU with those found experimentally. As seen in Figure 5 the simulated values of k_{app} increase with increasing alkane carbon number, but here again the predicted values of k_{app} lie well below those observed experimentally by a factor of 10 for propane and a factor of 100 for hexane. We believe that the most of this discrepancy is associated with the small cluster size (T5) used for the determination of k_{int}, which as shown for the case of MFI can results in apparent rate coefficients that are at least an order of magnitude smaller than those determined using a small cluster. An additional factor contributing to the discrepancy is the level of theory used for the calculation of k_{int}. Reference to Table 4 suggests that with an increase in the level of theory from DFT/B3LYP/SV(P) to DFT/M05-2X/6-311+G(2df,2p) or MP2/def2-TZVPP, the intrinsic activation energy would decrease by 30 to 37 kJ/mol. These differences translate into an additional increase in k_{app} of more than 100. Thus, we suggest that the discrepancy between predicted and measure values of k_{app} seen in Figure 5 is due to a combination of cluster size and level of theory used to determine k_{int}. The increase in the deviation between simulation and experiment with increasing alkane carbon number may also be due to an increasing contribution of bimolecular cracking to the experimental results, a phenomenon not described in the theoretical model of alkane cracking presented here.

Conclusions

We have shown that a simple model separating the intrinsic kinetics of alkane cracking from the thermodynamics of alkane adsorption provides a sound theoretical basis for estimating the apparent rate constants for alkane cracking. The thermodynamics of alkane adsorption can be calculated reliably from Monte Carlo simulation in the NVT framework, assuming a purely siliceous zeolite lattice. The localization of specific C−C bonds near Brønsted-acid sites where cracking occurs can also be determined from an analysis of the Monte Carlo simulations. The intrinsic rate coefficient for the cracking of specific C−C bonds in adsorbed alkanes can be calculated using density functional theory in combination with absolute rate theory. These calculations were carried out using a T5 cluster to represent the Brønsted acid site. While computationally tractable, the small cluster model does not account for the effects of dispersive interactions on the structure and energy of the reactant and transition states,[31−33] nor for the effects of acid centers present at next-nearest neighbor T sites. The simulations of alkane cracking in MFI and FAU reported here show good agreement with the observed effect of alkane chain length on the apparent rate coefficient for alkane cracking but are consistently lower in absolute value by a factor 10 to 100. This discrepancy is attributed for the most part to the use of a small cluster for the quantum chemical calculations and the level of theory used. This conclusion is supported by limited calculations done with a T23 cluster for the cracking on propane and butane on MFI. These calculations give values of the apparent activation energy for propane and butane cracking that agree very well with those observed experimentally and apparent rate coefficients for the cracking of these alkanes that are larger than those observed by only a factor of 3−4. The level of quantum chemical theory used also influences the magnitude of the apparent coefficient but to a lesser extent than cluster size. Our work also shows that the intrinsic and apparent rate coefficients for alkane cracking on MFI are higher than for cracking under identical conditions on FAU, which is in good agreement with recent experimental observations. A further finding is that intrinsic kinetics has a larger influence than adsorption thermodynamics on the chain length dependence of the rate of alkane cracking.

Acknowledgment. This work was supported in part by a grant from Chevron Energy and Technology Company. N. Hansen also wishes to acknowledge the Deutsche Forschungsgemeinschaft (DFG) in priority program SPP 1155 and the Norddeutscher Verbund für Hoch- und Höchstleistungsrechnen (HLRN) for computing time. J.S. wishes to acknowledge Dr. Jocelyn Rodgers for many helpful discussions.

Supporting Information Available: Discussion of statistical factors for rate constants. Details of CBMC simulations. Discussion of the distribution of $P_{react}(i,j)$. Energies and Cartesian coordinates of reactant and transition states. Detailed DFT results. This material is available free of charge via the Internet at http://pubs.acs.org.

References and Notes

(1) Dubbeldam, D.; Calero, S.; Vlugt, T. J. H.; Krishna, R.; Maesen, T. L. M.; Smit, B. United Atom Force Field for Alkanes In Nanoporous Materials. *J. Phys. Chem. B* **2004**, *108*, 12301–12313.

(2) Beerdsen, E.; Dubbeldam, D.; Smit, B. Understanding Diffusion in Nanoporous Materials. *Phys. Rev. Lett.* **2006**, *96*, 044501.

(3) Honkala, K.; Hellman, A.; Remediakis, I. N.; Logadottir, A.; Carlsson, A.; Dahl, S.; Christensen, C. H.; Nørskov, J. K. Ammonia Synthesis from First-Principles Calculations. *Science* **2005**, *307*, 555–558.

(4) Heyden, A.; Hansen, N.; Bell, A. T.; Keil, F. J. Nitrous Oxide Decomposition Over Fe-ZSM-5 in the Presence Of Nitric Oxide: A Comprehensive DFT Study. *J. Phys. Chem. B* **2006**, *110*, 17096–17114.

(5) Mei, D.; Sheth, P. A.; Neurock, M.; Smith, C. M. First-Principles-Based Kinetic Monte Carlo Simulation of the Selective Hydrogenation Of Acetylene Over Pd(111). *J. Catal.* **2006**, *242*, 1–15.

(6) Hafner, J. Adsorption and Reaction of Organic Molecules on Solid Surfaces - Ab-Initio Density Functional Investigations. *Monatsh. Chem.* **2008**, *139*, 373–387.

(7) Hansen, N.; Krishna, R.; van Baten, J. M.; Bell, A. T.; Keil, F. J. Analysis Of Diffusion Limitation in the Alkylation Of Benzene Over H-ZSM-5 by Combining Quantum Chemical Calculations, Molecular Simulations, and a Continuum Approach. *J. Phys. Chem. C* **2009**, *113*, 235–246.

(8) Vayssilov, G. N.; Aleksandrov, H. A.; Petrova, G. P.; Petkov, P. S. Computational Modeling of Nanoporous Materials. In *Ordered Porous Solids, Recent Advances and Prospects*; Valtchev, V., Mintova, S., Tsapatsis, M., Eds; Elsevier: Amsterdam, 2009; Vol. 1, pp 211−238.

(9) Broadbelt, L. J.; Snurr, R. Q. Applications Of Molecular Modeling in Heterogeneous Catalysis Research. *Appl. Catal., A* **2000**, *200*, 23–46.

(10) Maesen, T. L. M.; Calero, S.; Schenk, M.; Smit, B. Alkane Hydrocracking: Shape Selectivity Or Kinetics. *J. Catal.* **2004**, *221*, 241–251.

(11) Maesen, T. L. M.; Beerdsen, E.; Calero, S.; Dubbeldam, D.; Smit, B. Understanding Cage Effects in the N-Alkane Conversion On Zeolites. *J. Catal.* **2006**, *237*, 278–290.

(12) van Santen, R. A.; Offermans, W. K.; Malek, K.; Pidko, E. A. Computational Modeling of Catalytic Reactivity. *Mol. Simul.* **2007**, *33*, 327–336.

(13) Rigutto, M. S. In *Zeolites And Related Materials: Trends, Targets and Challenges*; Gedeon, A., Massiania, P., Babonneau, F., Eds; Elsevier: Amsterdam, 2008; Vol. 174, p 43−52.

(14) Greensfelder, B. S.; Voge, H. H.; Good, G. M. Catalytic and Thermal Cracking of Pure Hydrocarbons - Mechanisms of Reaction. *Ind. Eng. Chem. Res.* **1949**, *41*, 2573–2584.

(15) Thomas, C. L. Chemistry of Cracking Catalysts. *Ind. Eng. Chem. Res.* **1949**, *41*, 2564–2573.

(16) Haag, W. O.; Dessau, R. M. Duality of Mechanism for Acid-Catalyzed Paraffin Cracking. In *Proceedings of The Eighth International Congress On Catalysis*; Dechema: Frankfurt am Main, 1984; Vol 2, pp 305−316.

(17) Jentoft, F. C.; Gates, B. C. Solid-Acid-Catalyzed Alkane Cracking Mechanisms: Evidence from Reactions of Small Probe Molecules. *Top. Catal.* **1997**, *4*, 1–13.

(18) Kotrel, S.; Knözinger, H.; Gates, B. C. The Haag-Dessau Mechanism of Protolytic Cracking of Alkanes. *Microporous Mesoporous Mater.* **2000**, *35*−*6*, 11–20.

(19) Babitz, S. M.; Williams, B. A.; Miller, J. T.; Snurr, R. Q.; Haag, W. O.; Kung, H. H. Monomolecular Cracking of N-Hexane on Y, MOR, and ZSM-5 Zeolites. *Appl. Catal., A* **1999**, *179*, 71–86.

(20) Beyerlein, R. A.; McVicker, G. B.; Yacullo, L. N.; Ziemiak, J. J. Influence of Framework and Nonframework Aluminum on The Acidity of High-Silica, Proton-Exchanged Fau-Framework Zeolites. *J. Phys. Chem.* **1988**, *92*, 1967–1970.

(21) Fritz, P. O.; Lunsford, J. H. The Effect of Sodium Poisoning on Dealuminated Y-Type Zeolites. *J. Catal.* **1989**, *118*, 85–98.

(22) Haag, W. O.; Lago, R. M.; Weisz, P. B. The Active-Site of Acidic Aluminosilicate Catalysts. *Nature* **1984**, *309*, 589–591.

(23) Kotrel, S.; Rosynek, M. P.; Lunsford, J. H. Intrinsic Catalytic Cracking Activity of Hexane over H-ZSM-5, H-Beta And H-Y Zeolites. *J. Phys. Chem. B* **1999**, *103*, 818–824.

(24) Krannila, H.; Haag, W. O.; Gates, B. C. Monomolecular And Biomolecular Mechanisms of Paraffin Cracking - N-Butane Cracking Catalyzed By HZSM-5. *J. Catal.* **1992**, *135*, 115–124.

(25) Narbeshuber, T. F.; Vinek, H.; Lercher, J. A. Monomolecular Conversion of Light Alkanes over H-ZSM-5. *J. Catal.* **1995**, *157*, 388–395.

(26) Ramachandran, C. E.; Williams, B. A.; van Bokhoven, J. A.; Miller, J. T. Observation of a Compensation Relation for N-Hexane Adsorption in Zeolites with Different Structures: Implications for Catalytic Activity. *J. Catal.* **2005**, *233*, 100–108.

(27) van Bokhoven, J. A.; Williams, B. A.; Ji, W.; Koningsberger, D. C.; Kung, H. H.; Miller, J. T. Observation Of a Compensation Relation for Monomolecular Alkane Cracking by Zeolites: The Dominant Role of Reactant Sorption. *J. Catal.* **2004**, *224*, 50–59.

(28) Wei, J. Adsorption and Cracking of N-Alkanes Over ZSM-5: Negative Activation Energy Of Reaction. *Chem. Eng. Sci.* **1996**, *51*, 2995–2999.

(29) Xu, B.; Sievers, C.; Hong, S. B.; Prins, R.; van Bokhoven, J. A. Catalytic Activity of Bronsted Acid Sites in Zeolites: Intrinsic Activity, Rate-Limiting Step, and Influence of the Local Structure of the Acid Sites. *J. Catal.* **2006**, *244*, 163–168.

(30) Bhan, A.; Gounder, R.; Macht, J.; Iglesia, E. Entropy Considerations In Monomolecular Cracking of Alkanes on Acidic Zeolites. *J. Catal.* **2007**, *253*, 221–224.

(31) Hansen, N.; Kerber, T.; Sauer, J.; Bell, A. T.; Keil, F. J., *J. Am. Chem. Soc.*, submitted for publication.

(32) Svelle, S.; Tuma, C.; Rozanska, X.; Kerber, T.; Sauer, J. Quantum Chemical Modeling of Zeolite-Catalyzed Methylation Reactions: Toward Chemical Accuracy for Barriers. *J. Am. Chem. Soc.* **2009**, *131*, 816–825.

(33) Tuma, C.; Sauer, J. Treating Dispersion Effects in Extended Systems by Hybrid MP2: DFT Calculations - Protonation Of Isobutene In Zeolite Ferrierite. *Phys. Chem. Chem. Phys.* **2006**, *8*, 3955–3965.

(34) Olson, D. H.; Koktailo, G. T.; Lawton, S. L.; Meier, W. M. Crystal-Structure and Structure-Related Properties of ZSM-5. *J. Phys. Chem.* **1981**, *85*, 2238–2243.

(35) Olson, D. H.; Khosrovani, N.; Peters, A. W.; Toby, B. H. Crystal Structure Of Dehydrated Cszsm-5 (5.8A1): Evidence for Nonrandom Aluminum Distribution. *J. Phys. Chem. B* **2000**, *104*, 4844–4848.

(36) Barone, G.; Casella, G.; Giuffrida, S.; Duca, D. H-ZSM-5 Modified Zeolite: Quantum Chemical Models of Acidic Sites. *J. Phys. Chem. C* **2007**, *111*, 13033–13043.

(37) Mentzen, B. F.; Sacerdoteperonnet, M. Prediction of Preferred Proton Locations in H-MFI Benzene Complexes by Molecular Mechanics Calculations - Comparison with NMR, Structural and Calorimetric Results. *Mater. Res. Bull.* **1994**, *29*, 1341–1348.

(38) Brändle, M.; Sauer, J. Acidity Differences between Inorganic Solids Induced by Their Framework Structure. A Combined Quantum Mechanics Molecular Mechanics Ab Initio Study on Zeolites. *J. Am. Chem. Soc.* **1998**, *120*, 1556–1570.

(39) Ryder, J. A.; Chakraborty, A. K.; Bell, A. T. Density Functional Theory Study of Proton Mobility in Zeolites: Proton Migration and Hydrogen Exchange In ZSM-5. *J. Phys. Chem. B* **2000**, *104*, 6998–7011.

(40) Zygmunt, S. A.; Curtiss, L. A.; Zapol, P.; Iton, L. E. Ab Initio and Density Functional Study of the Activation Barrier for Ethane Cracking in Cluster Models of Zeolite H-ZSM-5. *J. Phys. Chem. B* **2000**, *104*, 1944–1949.

(41) Olson, D. H. The Crystal-Structure of Dehydrated NaX. *Zeolites* **1995**, *15*, 439–443.

(42) Ahlrichs, R.; Bär, M.; Häser, M.; Horn, H.; Kölmel, C. Electronic-Structure Calculations on Workstation Computers - The Program System Turbomole. *Chem. Phys. Lett.* **1989**, *162*, 165–169.

(43) Becke, A. D. Density-Functional Exchange-Energy Approximation with Correct Asymptotic-Behavior. *Phys. Rev. A: At., Mol., Opt. Phys.* **1988**, *38*, 3098–3100.

(44) Lee, C. T.; Yang, W. T.; Parr, R. G. Development of the Colle-Salvetti Correlation-Energy Formula into a Functional of the Electron-Density. *Phys. Rev. B.: Condens. Matter Mater. Phys.* **1988**, *37*, 785–789.

(45) Treutler, O.; Ahlrichs, R. Efficient Molecular Numerical-Integration Schemes. *J. Chem. Phys.* **1995**, *102*, 346–354.

(46) Schäfer, A.; Horn, H.; Ahlrichs, R. Fully Optimized Contracted Gaussian-Basis Sets for Atoms Li To Kr. *J. Chem. Phys.* **1992**, *97*, 2571–2577.

(47) Schäfer, A.; Huber, C.; Ahlrichs, R. Fully Optimized Contracted Gaussian-Basis Sets of Triple Zeta Valence Quality for Atoms Li To Kr. *J. Chem. Phys.* **1994**, *100*, 5829–5835.

(48) Weigend, F.; Furche, F.; Ahlrichs, R. Gaussian Basis Sets of Quadruple Zeta Valence Quality for Atoms H-Kr. *J. Chem. Phys.* **2003**, *119*, 12753–12762.

(49) Peters, B.; Heyden, A.; Bell, A. T.; Chakraborty, A. A Growing String Method for Determining Transition States: Comparison to the Nudged Elastic Band And String Methods. *J. Chem. Phys.* **2004**, *120*, 7877–7886.

(50) Baker, J. An Algorithm For The Location of Transition-States. *J. Comput. Chem.* **1986**, *7*, 385–395.

(51) Zhao, Y.; Truhlar, D. G. A Density Functional That Accounts for Medium-Range Correlation Energies in Organic Chemistry. *Org. Lett.* **2006**, *8*, 5753–5755.

(52) Zhao, Y.; Truhlar, D. G. Benchmark Data for Interactions in Zeolite Model Complexes and Their Use for Assessment and Validation of Electronic Structure Methods. *J. Phys. Chem. C* **2008**, *112*, 6860–6868.

(53) Zhao, Y.; Schultz, N. E.; Truhlar, D. G. Design of Density Functionals By Combining the Method Of Constraint Satisfaction With Parametrization For Thermochemistry, Thermochemical Kinetics, and Noncovalent Interactions. *J. Chem. Theory Comput.* **2006**, *2*, 364–382.

(54) Zhao, Y.; Truhlar, D. G. Density Functionals with Broad Applicability in Chemistry. *Acc. Chem. Res.* **2008**, *41*, 157–167.

(55) Frisch, M. J.; Trucks, G. W.; Schlegel, H. B.; Scuseria, G. E.; Robb, M. A.; Cheeseman, J. R.; Montgomery, J. A.; Vreven, T.; Kudin, K. N.; Burant, J. C.; Millam, J. M.; Iyengar, S. S.; Tomasi, J.; Barone, V.; Mennucci, B.; Cossi, M.; Scalmani, G.; Rega, N.; Petersson, G. A.; Nakatsuji, H.; Hada, M.; Ehara, M.; Toyota, K.; Fukuda, R.; Hasegawa, J.; Ishida, M.; Nakajima, T.; Honda, Y.; Kitao, O.; Nakai, H.; Klene, M.; Li, X.; Knox, J. E.; Hratchian, H. P.; Cross, J. B.; Bakken, V.; Adamo, C.; Jaramillo, J.; Gomperts, R.; Stratmann, R. E.; Yazyev, O.; Austin, A. J.; Cammi, R.; Pomelli, C.; Ochterski, J. W.; Ayala, P. Y.; Morokuma, K.; Voth, G. A.; Salvador, P.; Dannenberg, J. J.; Zakrzewski, V. G.; Dapprich, S.; Daniels, A. D.; Strain, M. C.; Farkas, O.; Malick, D. K.; Rabuck, A. D.; Raghavachari, K.; Foresman, J. B.; Ortiz, J. V.; Cui, Q.; Baboul, A. G.; Clifford, S.; Cioslowski, J.; Stefanov, B. B.; Liu, G.; Liashenko, A.; Piskorz, P.; Komaromi, I.; Martin, R. L.; Fox, D. J.; Keith, T.; Laham, A.; Peng,

C. Y.; Nanayakkara, A.; Challacombe, M.; Gill, P. M. W.; Johnson, B.; Chen, W.; Wong, M. W.; Gonzalez, C.; Pople, J. A. *Gaussian 03*, Revision E.01; Gaussian, Inc.: Wallingford, CT, 2003.

(56) Krishnan, R.; Binkley, J. S.; Seeger, R.; Pople, J. A. Self-Consistent Molecular-Orbital Methods. XX. Basis Set for Correlated Wave-Functions. *J. Chem. Phys.* **1980**, *72*, 650–654.

(57) McLean, A. D.; Chandler, G. S. Contracted Gaussian-Basis Sets for Molecular Calculations. I. 2Nd Row Atoms Z=11−18. *J. Chem. Phys.* **1980**, *72*, 5639–5648.

(58) Weigend, F.; Ahlrichs, R. Balanced Basis Sets of Split Valence, Triple Zeta Valence and Quadruple Zeta Valence Quality for H to Rn: Design and Assessment of Accuracy. *Phys. Chem. Chem. Phys.* **2005**, *7*, 3297–3305.

(59) Hättig, C. Geometry Optimizations with The Coupled-Cluster Model CC2 Using the Resolution-of-the-Identity Approximation. *J. Chem. Phys.* **2003**, *118*, 7751–7761.

(60) Hättig, C.; Hellweg, A.; Köhn, A. Distributed Memory Parallel Implementation of Energies and Gradients for Second-Order Møller-Plesset Perturbation Theory with the Resolution-of-the-Identity Approximation. *Phys. Chem. Chem. Phys.* **2006**, *8*, 1159–1169.

(61) Baerends, E. J.; Ellis, D. S.; Ros, P. Self-Consistent Molecular Hartree-Fock-Slater Calculations - I. The Computational Procedure. *Chem. Phys.* **1973**, *2*, 41–51.

(62) Vahtras, O.; Almlöf, J.; Feyereisen, M. W. Integral Approximations For LCAO-SCF Calculations. *Chem. Phys. Lett.* **1993**, *213*, 514–518.

(63) Whitten, J. L. Coulombic Potential-Energy Integrals and Approximations. *J. Chem. Phys.* **1973**, *58*, 4496–4501.

(64) Weigend, F.; Haser, M.; Patzelt, H.; Ahlrichs, R. RI-MP2: Optimized Auxiliary Basis Sets and Demonstration of Efficiency. *Chem. Phys. Lett.* **1998**, *294*, 143–152.

(65) Kresse, G.; Hafner, J. Ab Initio Molecular Dynamics for Open-Shell Transition Metals. *Phys. Rev. B* **1993**, *48*, 13115–13126.

(66) Kresse, G.; Hafner, J. Ab Initio Molecular-Dynamics Simulation of the Liquid-Metal-Amorphous-Semiconductor Transition in Germanium. *Phys. Rev. B* **1993**, *49*, 14251–14296.

(67) Kresse, G.; Furthmüller, J. Efficiency of Ab-Initio Total Energy Calculations for Metals and Semiconductors Using a Plane-Wave Basis Set. *J. Comput. Mater. Sci.* **1996**, *6*, 15–50.

(68) Kresse, G.; Furthmüller, J. Efficient Iterative Schemes for Ab Initio Total Energy Calculations Using a Plane Wave Basis Set. *Phys. Rev. B* **1996**, *54*, 11169–11186.

(69) Evans, M. G.; Polanyi, M. Some Applications of the Transition State Method to the Calculation of Reaction Velocities, Especially in Solution. *Trans. Faraday Soc.* **1935**, *31*, 875–894.

(70) Eyring, H. The Activated Complex in Chemical Reactions. *J. Chem. Phys.* **1935**, *3*, 107–115.

(71) McQuarrie, D. A. *Statistical Mechanics*, 1st ed.; Harper Collins: New York, 1973.

(72) Eder, F.; Lercher, J. A. Alkane Sorption In Molecular Sieves: The Contribution of Ordering, Intermolecular Interactions, and Sorption on Brønsted Acid Sites. *Zeolites* **1997**, *18*, 75–81.

(73) Narbeshuber, T. F.; Brait, A.; Seshan, K.; Lercher, J. A. The Influence of Extraframework Aluminum on H-FAU Catalyzed Cracking of Light Alkanes. *Appl. Catal., A* **1996**, *146*, 119–129.

(74) Katada, N.; Suzuki, K.; Noda, T.; Miyatani, W.; Taniguchi, F.; Niwa, M. Correlation of the Cracking Activity with Solid Acidity and Adsorption Property on Zeolites. *Appl. Catal., A* **2010**, *373*.

(75) Zhao, Y.; Truhlar, D. G. Design of Density Functionals That Are Broadly Accurate for Thermochemistry, Thermochemical Kinetics, and Nonbonded Interactions. *J. Phys. Chem. A* **2005**, *109*, 5656–5667.

(76) Denayer, J. F.; Souverijns, W.; Jacobs, P. A.; Martens, J. A.; Baron, G. V. High-Temperature Low-Pressure Adsorption of Branched C-5-C-8 Alkanes on Zeolite Beta, ZSM-5, ZSM-22, Zeolite Y, and Mordenite. *J. Phys. Chem. B* **1998**, *102*, 4588–4597.

(77) Sun, M. S.; Shah, D. B.; Xu, H. H.; Talu, O. Adsorption Equilibria of C-1 To C-4 Alkanes, CO_2, and SF_6 on Silicalite. *J. Phys. Chem. B* **1998**, *102*, 1466–1473.

JP101262Y